HHS Public Access

Author manuscript

ACS Catal. Author manuscript; available in PMC 2021 May 26.

Published in final edited form as:

ACS Catal. 2019 February 1; 9(2): 1329–1336. doi:10.1021/acscatal.8b04324.

Exploring the Catalytic Mechanism of Cas9 Using Information Inferred from Endonuclease VII

Hanwool Yoon, **Li Na Zhao**, **Arieh Warshel***

Department of Chemistry, University of Southern California, 418 SGM Building, 3620 McClintock Ave, Los Angeles, California 90089-1062, United States

Abstract

Elucidating the nature of the gene editing mechanism of CRISPR (Clustered Regularly Interspaced Short Palindromic Repeats) is an important task in view of the role of this breakthrough to the advancement of human medicine. In particular, it is crucial to understand the catalytic mechanism of Cas9 (one of the CRISPR associated proteins) and its role in confirming accurate editing. Thus, we focus in this work on an attempt to analyze the catalytic mechanism of Cas9. Considering the absence of detailed structural information on the active form of Cas9, we use an empirical valence bond (EVB) which is calibrated on the closely related mechanism of T4 endonuclease VII. The calibrated EVB is then used in studying the reaction of Cas9, while trying several structural models. It is found that the catalytic activation requires a large conformational change, where K848 or other positively charged group moves from a relatively large distance toward the scissile phosphate. This conformational change leads to the change in position of the Mg^{2+} ion and to a major reduction in the activation barrier for the catalytic reaction. Our finding provides an important clue on the nature of the catalytic activation of CAS9 and thus should help in elucidating a key aspect of the gene editing process. For example, the approach used here should be effective in exploring the nature of off target activation and its relationship to the energetics of the unwinding process. This strategy may offer ways to improve the selectivity of Cas9.

Graphical Abstract

*Corresponding Author: warshel@usc.edu.

The authors declare no competing financial interest.

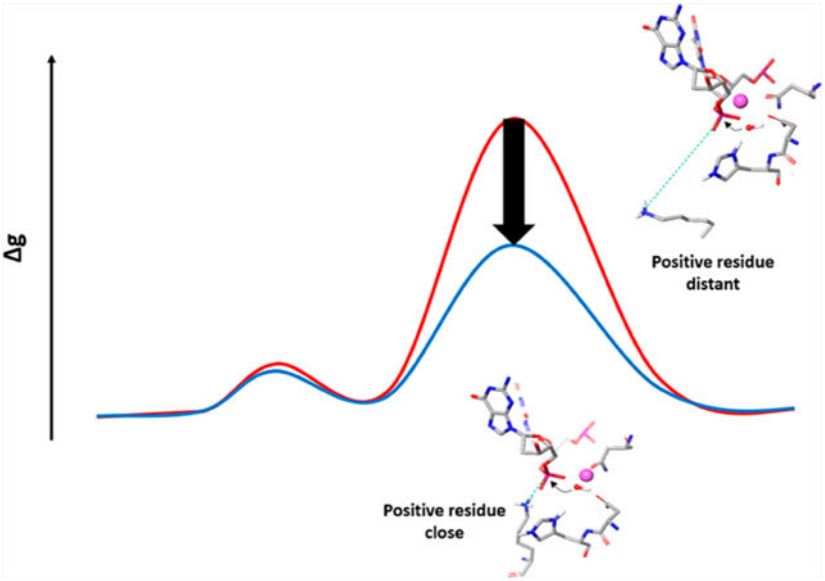

Keywords

CRISPR; Cas9; catalysis; EVB; nucleases

1. INTRODUCTION

The CRISPR (Clustered Regularly Interspaced Short Palindromic Repeats)–Cas (CRISPR-associated genes) system has recently received major attention for its remarkable applicability in gene editing.[1] Cas9, one of the CRISPR associated proteins, is an RNA-guided DNA endonuclease enzyme which was originally found in the adaptive immune system of *Streptococcus pyogenes*.[2] The editing action of Cas9 (described schematically in Figure 1) starts where the native Cas9 endonuclease binds to a guide RNA composed of two RNAs, CRISPR RNA(crRNA) and a trans-activating RNA-(tracrRNA),[3] where the system has been simplified (relative to the Cas9 that uses in nature the separate crRNA and tracrRNA) by replacing these two disparate RNAs with a single guide RNA (sgRNA).[2] After a conformational change that transfers the Cas9 complex with the guide RNA to its activated form, the complex searches for a target DNA with sequences that match the conserved protospacer adjacent motif (PAM) sequence, which is responsible for binding of the target DNA to the Cas9-guid RNA complex.[4] The double stranded DNA (dsDNA) is melted when the Cas9 protein finds a target sequence in the PAM region and an RNA–DNA formation is hybridized.[5] At this stage, the well-conserved RuvC and HNH domains cleave the non-target and the target DNA strand, respectively. The elucidation of the details of the mechanism of the type II CRISPR is an area of a very active research. There have been many structural studies that identified the conformational changes in different steps of the DNA binding,[6] the PAM recognition,[5,7] the transformation of the cleavage domains to the precatalytic state,[8] and subsequent cleavage.[9] These structural studies suggested that conformational changes of the HNH domain play important roles in the activation process. In particular, after the dsDNA binding and R-loop formation, a significant conformational rearrangement of the

HNH domain brings this region close to the cleavage site on the target strand (Figure 1).[10] An early experiment using intramolecular Förster Resonance Energy Transfer (FRET) revealed that the conformational dynamics of the HNH domain plays an important role in controlling the cleavage efficiency.[8c] However, this high flexibility of the HNH domain makes it difficult to determine the precise catalytically active structure, and the exact mechanism of the catalysis is still elusive. The difference in the conformation and position of the HNH domain in the two available Cas9 structures (with an incomplete non-target DNA strand[5] and with both unwound DNA strands[10]) demonstrated the plasticity of the HNH domain and its important interplay with the nucleic acids. However, even in the latter structures, in the absence of divalent cations, the distance between the catalytic HIS840 and the scissile phosphate is ~10 Å, which is still too far to support the catalytic reaction.

There have been several *in sillico* attempts of using extensive molecular dynamic simulations in exploring possible active conformations.[11] Furthermore, a recent cryo-EM structure, solved at a 5.2 Å resolution, was used in MD simulation that tried to determine the closest position of the HNH domain to the cleavage site.[8b] However, the relevance and validity of those structures cannot be established without calculating the free energy of the chemical reaction that would occur in the corresponding structures.

At this stage, in the absence of a high resolution structure of a catalytically active state, it may be still too early to try to examine in a conclusive way the free energy landscape of the catalytic process. However, in view of the importance of the understanding of the Cas9 action, we move in this direction by modeling the catalysis with several structural hypotheses. In particular, our previous computational studies for polymerases and endonucleases provide a powerful benchmark as all of these systems share very similar chemistry.

In view of the uncertainties about the catalytic structure of Cas9, it is important to exploit relevant information from other related systems. In this respect, we noted that the HNH domain shares structural similarity with other nucleases such as Staphylococcal nuclease,[12] and especially with phage T4 endonuclease VII[13](Endo VII, rmsd of 2.7 Å for 61 equiv Cα atoms) and *Vibrio vulnificus* nuclease[14] (rmsd of 2.7 Å for 77 Cα atoms). While the catalytic structure at high resolution for Cas9 has not been reported yet, most of the other nucleases including the ones mentioned above are known to have one metal ion mechanism (Figure 2) and have similar conformations for the catalytic state, which includes a histidine/glutamic acid as a general base, aspartic acid or/and asparagine to hold a divalent cation, and positively charged residues nearby. One major difference between these nucleases and the currently assumed catalytic state of Cas9 (from Cryo-EM structure (PDB: 5Y36)[8b] and those suggested by molecular dynamic simulations[11b,c]) is a positively charged residue on the other side of the divalent cation ion and next to the O3′ of the scissile phosphate. For example, there is ARG87 in Staphylococcal nuclease (Figure2a), H43 in Endo VII (Figure 2b), and ARG99 in Endonuclease Vvn (Figure 2c). In the case of Endo VII, the H43T mutant has shown a very low activity.[15] Therefore, it seems that the presence of a positive charge has a significant role for the common catalysis.

Neither the Cryo-EM structure nor other FRET experiment for Cas9 has shown any corresponding positive residue nearby. However, the HNH domain is known to have major conformational changes right before the cleavage event.[8a,c,16] Looking for possible positive residues, we note that there are only two positive residues (K848 and K855) within 10 Å from the scissile phosphate. Interestingly, these two residues were mutated to alanine to improve the specificity of Cas9 (eSpCas9 1.1[17]) and are widely used to avoid off-target cleavages. Although this mutant still has cleavage activity unlike Endo VII, it was reported that it has slower cleavage rates.[16] Thus, we explore here the possible catalytic role for these two residues. This is done considering several structural options with the hope to get an insight about the activation process.

Significantly, our study finds that moving K848 near the reaction center leads to a major structural change and to a very large rate acceleration. This structural change has most probably a major role in translating changes in base pairing to the activation of Cas9.

2. METHODS

Our calculations of the activation barriers were performed using the empirical valence-bond (EVB) method[18] that has been used in many of our previous studies, which successfully quantified the key factors in enzyme catalysis (e.g., ref 19). Furthermore, our EVB studies have revealed the important factors that lead to the high replication fidelity of DNA polymerase β.[20]

All the calculations in this study used the MOLARIS-XG package.[21] The reacting region and the Cas9–RNA–DNA complex for the EVB calculations were immersed in a 30 Å sphere of water molecules using the surface-constraint all-atom solvent (SCAAS) type boundary condition.[21a] This system was further surrounded by a 2 Å surface of Langevin dipoles and then a bulk continuum. The local reaction field (LRF) method[21a] was used to treat the long-range effects. All other atoms beyond this sphere were fixed at their initial positions in the Cryo-EM structure, and the electrostatic interaction from outside of the sphere was turned off. The center of the simulation sphere was set to the geometric center of the EVB reacting atoms with the same parameters defined in our previous study of Staphylococcal nuclease[24] (see however below the treatment of the histidine parameters). The protonation states were determined by calculating the pK_a's with our coarse grained (CG) model[22] for the residue within 12 Å from the center of the simulation with a macroscopic large charge dielectric for the effect of ionizable residues beyond this range.

After this preparation of the system, the structure was equilibrated by increasing the temperature from 10 K to 300 K for the first 200 ps with a 100 kcal/mol $Å^2$ positional constraint on each atom. The constraint was gradually released over the next 100 ps. The system was then relaxed for 10 ns, followed by generating five different starting structures with 40 ps of consecutive relaxation from the previous structures. The average of each free energy calculation from the five runs with each of these starting structures is reported as the results. The EVB free energy calculations used the free energy perturbation/umbrella sampling approach (FEP/US)[18c] with 51 frames of 10 ps each and 1 fs time step. Note that the starting structures were relaxed with histidine protonated at both δ and ε positions and a

hydroxide ion. In the first calculation, the histidine transferred a proton to the hydroxide; then, the opposite sign was applied to get the free energy of the protonation on the histidine. In the second calculation starting from the same relaxed structures as the one used for the proton transfer, the EVB potential was changed from the reactant to the intermediate potential. The reaction regions were extracted at each 10 fs of the simulation with the scissile phosphate converted to dimethyl phosphate and then solvated for 2.5 ps while the EVB reacting atoms were fixed. This simulation was used to calibrate the gas phase shift and the off diagonal term of the EVB Hamiltonian.

The stepwise associative mechanism was considered, as our previous study[23] proved that it is more practical to explore the TS free energy with the well-defined penta-covalent intermediate state between the nucleophilic attack and the bond breaking steps, while it gives a similar result to that of the concerted mechanism. Since we focus on the overall cleavage barrier, the calibration step for the barrier of the protonation step and the EVB calculation of the bond breaking steps were omitted.

3. RESULTS AND DISCUSSION

3.a. EVB Simulations of the Reaction of T4 Endonuclease VII.

Before exploring the reaction in Cas9, we explored the same reaction for T4 Endonucleases VII (Endo VII). The study of Endo VII was based on trying to reproduce the observed kinetics, considering the mechanism depicted in Figure 3 and using the same EVB parameters from the previous study for Staphylococcal nuclease[24] for the one metal mechanism. We note, however, that unlike Staphylococcal nuclease that uses GLU43 as a base, Endo VII and Cas9 use histidine to abstract proton from a water molecule. The proton was transferred to the δ nitrogen of H41, and the partial charges and vdW parameters of HIP and HIE for the EVB were taken from MOLARIS's force field. The gas phase shift was calibrated according to the free energy of proton transfer, obtained from the pK_a of histidine and water.

The crystal structure of H43A (PDB: 2QNC), which is catalytically inactive, was used. For the wild type, H43A was mutated back to a histidine. In the original structure, the position of the Mg^{2+} ion is coordinated between OP1 and O3′ of the scissile phosphate (Figure 4a). Although the EVB results for nucleophilic attack by OH^- were reasonable, using this coordination of the Mg^{2+}, there was a very large free energy cost (~15 kcal/mol) for the proton transfer step, because the distance between OH^- and the Mg^{2+} was too far to benefit the negative charge on the oxygen as it is deprotonated. This effect of the magnesium on the proton transfer step has been already observed in many of our previous studies of DNA polymerases.[20c,23a,25] Thus, the structure was equilibrated with a constraint that positioned the Mg^{2+} ion in a way that favored the proton transfer step as well as the nucleophilic attack step (Figure 4b). Interestingly, when the Cas9 structure was relaxed with HIS840 brought close to the active site, the Mg^{2+} ion was also positioned between OP1 of the scissile phosphate and the attacking OH^-. We note that although our calculations considered the OH^- in the first coordination shell of the Mg^{2+} ion, it is also possible that this ion resides in the first or second shell. This is an important challenging open question, but it is assumed

that a calibration on Endo VII does provide a reasonable result even without resolving this question.

The above generated structure was equilibrated slowly and relaxed for 1 ns, and the EVB was then calculated (Figure 5 and Table 1). The observed k_{cat} was nicely reproduced for the wild type, while H43A showed a very high free energy barrier.

3.b. EVB Calculations of the Reaction of Cas9.

After reproducing the kinetics of Endo VII, we used the same structural preparation and settings in calculating the same reaction for Cas9. In choosing the structure, we noted the recent Cryo-EM structure (PDB: 5Y36), which was recently reported as the closest conformation to the catalytic state. However, this structure is likely to be far from the actual catalytic structure, since the position of the histidine base (which was mutated to alanine to inactivate the enzyme) is located ~8 Å away from the scissile phosphate. Moreover, N863, which corresponds to N62 in Endo VII, which is clearly a catalytic residue (since its mutation to alanine also causes inactivity), is ~10 Å away from the catalytic site. Thus, we applied distance constraints with a 15 kcal/mol $Å^2$ force constant, at 2.0 Å between the OD1 of N863 and Mg^{2+} and at 5.0 Å between the CG of H840 and the phosphorus of the scissile phosphate, and the structures were relaxed for 10 ns (Figure 6).

In exploring the possible role of a positive residue near the catalytic site, we identified two potential residues (LYS848 and K855) within 10 Å from this site. In addition, we identified K810 that is, however, at a distance of ~15 Å (the possible involvement of this residue is discussed in the Conclusions section). While the side chain of K848 is highly flexible and can be moved toward the catalytic site, K855 could not be brought to the site even with a distance constraint with a 50 kcal/mol $Å^2$ force constant, due to the presence of other residues on the way. Thus, we took the structure prepared above and imposed a distance constraint with a 10 kcal/mol $Å^2$ force constant at 2.0 Å between the NZ of K848 and the O3′ of the scissile phosphate and pulled the lysine next to the phosphate during 200 ps of relaxation (Figure 7).

The following three cases were explored: (a) K848 is kept far from the scissile phosphate, as in its the original structure, (b) K848 is brought near to the scissile phosphate but is not ionized, and (c) the ionized K848 is brought near the scissile phosphate (Figure 8 and Table 2). We compared our EVB barrier to the barrier obtained from a recent study, where the intrinsic rate of cleavage by the HNH domain was determined to be 0.67 s^{-1}.[26] The calculated barrier was found to be higher when K848 was far away (both for the PT step and nucleophilic attack step) than when it was near the catalytic site. When we ionized the K848, the barrier was reduced by about 5 kcal/mol relative to the case when it was not ionized, and most of the reduction was at the nucleophilic attack step. However, the change in barrier upon uncharging K848 is much smaller than the overall change upon conformational change. Thus, the main change is not due to the charge of K848 but to other structural changes. Exploring this effect, we found that it is largely due to the motion of the Mg^{2+} ion, which changes drastically the exothermicity of the proton transfer step. More specifically, the Mg^{2+} moved more closely to the O1A of the phosphate and the attacking OH^-, upon the

motion of K848, while the Mg^{2+} tries to interact with both the attacking OH^- and the O3A of the phosphate with a similar distance to that of K848 in the other case (Figure 7).

3.c. EVB Calculation for Cas9 with Mismatches around the Cleavage Site.

In view of the importance of controlling off target cleavage, we tried to explore the effect of mismatches around the cleavage site and the possible coupling to K848. The experiments with the engineered Cas9 and mismatches show that both the wild type and eCas9 are sensitive to mismatches around the cleavage site, which show almost no cleavage.[17,26] However, this sensitivity was found to be associated with an unwinding process. In our simulations, we converted 5′-GAA-3′ bases at 4,5,6 upstream positions of the PAM region in the target strand to 5′-AGG3′ bases and relaxed the system for 1 ns. This was followed by the same EVB calculations as before. Apparently, the mismatches did not change the barrier of the wild type significantly, while K848A shows a high barrier (Figure 9). While this result may look inconsistent with the experimental findings, it is in fact very reasonable. That is, the catalytic effect is obtained here with K848 near the reactive center. But this effect is unlikely to occur since the conformation with the mismatches is not likely to allow K848 to reach the reacting bonds (the needed unwinding is unlikely to be allowed as implied very clearly by the experimental study of ref 26). It is also possible that in this case we have incompetent DNA binding as the four consecutive PAM proximal mismatches showed almost no binding.[26] We look forward to having crystal structures with mismatches that would allow us to explore better the corresponding effect on catalysis, but we suspect that the hindered unwinding might block the conformational change which accompanies the movement of a positively charged residue to the neighborhood of the cleavage site.

4. CONCLUSIONS

Understanding the gene editing mechanism of CRISPR is a challenge of major importance in view of the crucial importance of gene therapy to medical advances. In this respect, it is crucial to understand the catalytic mechanism of Cas9 and its role in confirming accurate editing.

This work attempted to explore the energetics and mechanism of the chemical step in the activation of Cas9. Considering the absence of direct high resolution structural information on the catalytic configuration of Cas9, we first studied the closely related catalytic reaction of endonuclease VII. The EVB parameters obtained from the Endo VII study were then used in the simulations of Cas9. It was found that the most likely catalytic configuration involves a structure where a Lys residue comes close to the scissile phosphate. Obviously, this interesting conclusion needs more direct confirmations.

It is useful to further address the possible correlation of our cleavage mechanism with recent experimental observations.[26] This involves the following: (1) The engineered Cas9, namely eCas9 (K848A, K1003A, R1060A), has a slower cleavage rate than the WT. (2) The DNA unwinding takes place followed by the movement of the HNH domain toward the catalytic site. (3) There is a strong correlation between the DNA unwinding and the cleavage rate as the cleavage reaction proceeds more often in the unwound state. (4) The DNA unwinding is hindered by the mutation of positive residues in eCas9 and the PAM-distal DNA-RNA base

mismatches. (5) The impact of PAM-distal mismatches is greater for eCas9. Thus, they suggested that the enhancement in the cleavage specificity of eCas9 is largely due to destabilization of the unwound states by mutating the positive residues. While the results of the present work cannot be directly compared to the results obtained with eCas9, since we only mutated K848 and provide a clear mechanism of specificity, our results correspond to the same slower reaction rate in the absence of K848, suggesting the possible presence of a positive residue such as K848 near the cleavage site. In fact, Figure 4d of ref 26 shows a nearly constant difference in the cleavage rate between the WT and eCas9 above an unwound fraction of 50%. While different dynamics and DNA unwound fractions between the WT and eCas9 seem to be correlated with the specificity, it also seems that there is a constant factor that makes a difference at the cleavage stage regardless of the mismatches. Therefore, after the DNA unwinding, we hypothesize that the following conformational change of the HNH domain may position one of the positive residues mutated in eCas9 around the catalytic site. Interestingly, a recent study with long time scale MD simulation[11a] showed that K810 (another lysine known to reduce off-target cleavage)[17] is located around the phosphate-4 after 10 μs of simulation time. This observation further supports our hypothesis, although it is not clear whether the effect found with K848 will be obtained with K810. In fact, two different versions of eCas9 in the original proposal by Slaymaker et al.,[17] one with K848A and the other with K810A, both showed reduced off-target efficiencies.

At this point, it might be useful to discuss the frequent implications[8c,27] that the activation of Cas9 is controlled by dynamical processes and/or conformational control. First, with regard to the dynamical idea, as we argued frequently (e.g., ref 28), the rate of overcoming the activation barrier obeys in most cases the Boltzmann law, and the corresponding rate constants can be described by transition state theory (sometimes with a transmission factor correction). With regard to the conformational control, it is possible that the conformational barrier is slightly higher than the chemical barrier (difference in rate of a factor of around 3 (ref 27a)), although another recent experiment[26] showed a slower cleavage rate. However, as clarified in our discussion of the fidelity of DNA polymerase,[29] the modulation by conformational changes only occurs after evolution found a way to reduce the very high chemical activation barrier. Thus, it is unlikely that the conformational barrier controls the editing process.

Our preliminary exploration of the effect of changing bases did not involve the examination of the corresponding unwinding effect, which is found experimentally to be correlated with the catalytic activity. Although this finding may look puzzling, it is, in fact, consistent with the experimental observation (no unwinding, no catalysis). Combining studies of the melting dependence on the base pairs with EVB studies should provide a tool for refining the editing process. Of course, such a study will involve significant convergence problems, but we believe that advances in structural studies will help to make such studies reasonably reliable.

ACKNOWLEDGMENTS

We thank the University of Southern California High Performance Computing and Communication Center for computational resources. This work was supported by National Science Foundation Grant MCB 1707167, National Institute of Health R01-AI055926, and an A*STAR International Fellowship to L.N.Z.

REFERENCES

(1). (a)Wright AV; Nunez JK; Doudna JA Biology and Applications of CRISPR Systems: Harnessing Nature's Toolbox for Genome Engineering. Cell 2016, 164, 29–44. [PubMed: 26771484] (b)Doudna JA; Charpentier E The new frontier of genome engineering with CRISPR-Cas9. Science 2014, 346, 1258096. [PubMed: 25430774]

(2). Jinek M; Chylinski K; Fonfara I; Hauer M; Doudna JA; Charpentier E A Programmable Dual-RNA-Guided DNA Endonuclease in Adaptive Bacterial Immunity. Science 2012, 337, 816–821. [PubMed: 22745249]

(3). Deltcheva E; Chylinski K; Sharma CM; Gonzales K; Chao YJ; Pirzada ZA; Eckert MR; Vogel J; Charpentier E CRISPR RNA maturation by trans-encoded small RNA and host factor RNase III. Nature 2011, 471, 602–607. [PubMed: 21455174]

(4). Sternberg SH; Redding S; Jinek M; Greene EC; Doudna JA DNA interrogation by the CRISPR RNA-guided endonuclease Cas9. Nature 2014, 507, 62–67. [PubMed: 24476820]

(5). Anders C; Niewoehner O; Duerst A; Jinek M Structural basis of PAM-dependent target DNA recognition by the Cas9 endonuclease. Nature 2014, 513, 569–573. [PubMed: 25079318]

(6). Jinek M; Jiang FG; Taylor DW; Sternberg SH; Kaya E; Ma EB; Anders C; Hauer M; Zhou KH; Lin S; Kaplan M; Iavarone AT; Charpentier E; Nogales E; Doudna JA Structures of Cas9 Endonucleases Reveal RNA-Mediated Conformational Activation. Science 2014, 343, 1247997. [PubMed: 24505130]

(7). (a)Nishimasu H; Cong L; Yan WX; Ran FA; Zetsche B; Li YQ; Kurabayashi A; Ishitani R; Zhang F; Nureki O Crystal Structure of Staphylococcus aureus Cas9. Cell 2015, 162, 1113–1126. [PubMed: 26317473] (b)Nishimasu H; Ran FA; Hsu PD; Konermann S; Shehata SI; Dohmae N; Ishitani R; Zhang F; Nureki O Crystal Structure of Cas9 in Complex with Guide RNA and Target DNA. Cell 2014, 156, 935–949. [PubMed: 24529477]

(8). (a)Dagdas YS; Chen JS; Sternberg SH; Doudna JA; Yildiz A A conformational checkpoint between DNA binding and cleavage by CRISPR-Cas9. Sci. Adv 2017, 3, eaao0027. [PubMed: 28808686] (b)Huai C; Li G; Yao RJ; Zhang Y; Cao M; Kong LL; Jia CQ; Yuan H; Chen HY; Lu DR; Huang Q Structural insights into DNA cleavage activation of CRISPR-Cas9 system. Nat. Commun 2017, 8, 1375. [PubMed: 29123204] (c)Sternberg SH; LaFrance B; Kaplan M; Doudna JA Conformational control of DNA target cleavage by CRISPR-Cas9. Nature 2015, 527, 110–113. [PubMed: 26524520]

(9). Tangprasertchai NS; Di Felice R; Zhang XJ; Slaymaker IM; Vazquez Reyes C; Jiang W; Rohs R; Qin PZ CRISPR-Cas9Mediated DNA Unwinding Detected Using Site-Directed Spin Labeling. ACS Chem. Biol 2017, 12, 1489–1493. [PubMed: 28437608]

(10). Jiang FG; Taylor DW; Chen JS; Kornfeld JE; Zhou KH; Thompson AJ; Nogales E; Doudna JA Structures of a CRISPR-Cas9 R-loop complex primed for DNA cleavage. Science 2016, 351, 867–871. [PubMed: 26841432]

(11). (a)Palermo G; Chen JS; Ricci CG; Rivalta I; Jinek M; Batista VS; Doudna JA; McCammon JA Key role of the REC lobe during CRISPR–Cas9 activation by 'sensing', 'regulating', and 'locking' the catalytic HNH domain. Q. Rev. Biophys 2018, 51, e9.(b)Palermo G; Miao YL; Walker RC; Jinek M; McCammon JA CRISPR-Cas9 conformational activation as elucidated from enhanced molecular simulations. Proc. Natl. Acad. Sci. U. S. A 2017, 114, 7260–7265. [PubMed: 28652374] (c)Zuo ZC; Liu J Structure and Dynamics of Cas9 HNH Domain Catalytic State. Sci. Rep 2017, 7, 17271. [PubMed: 29222528]

(12). Cotton FA; Hazen EE; Legg MJ Staphylococcal Nuclease - Proposed Mechanism of Action Based on Structure of Enzyme-Thymidine 3′,5′-Bisphosphate-Calcium Ion Complex at 1.5-a Resolution. Proc. Natl. Acad. Sci. U. S. A 1979, 76, 2551–2555. [PubMed: 288045]

(13). Biertumpfel C; Yang W; Suck D Crystal structure of T4 endonuclease VII resolving a Holliday junction. Nature 2007, 449, 616–620. [PubMed: 17873859]

(14). Li CL; Hor LI; Chang ZF; Tsai LC; Yang WZ; Yuan HS DNA binding and cleavage by the periplasmic nuclease Vvn: a novel structure with a known active site. EMBO J. 2003, 22, 4014–4025. [PubMed: 12881435]

(15). GiraudPanis MJE; Lilley DMJ T4 endonuclease VII - Importance of a histidine-aspartate cluster within the zinc-binding domain. J. Biol. Chem 1996, 271, 33148–33155. [PubMed: 8955164]

(16). Yang MY; Peng SJ; Sun RR; Lin JD; Wang N; Chen CL The Conformational Dynamics of Cas9 Governing DNA Cleavage Are Revealed by Single-Molecule FRET. Cell Rep. 2018, 22, 372–382. [PubMed: 29320734]

(17). Slaymaker IM; Gao LY; Zetsche B; Scott DA; Yan WX; Zhang F Rationally engineered Cas9 nucleases with improved specificity. Science 2016, 351, 84–88. [PubMed: 26628643]

(18). (a)Warshel A; Weiss RM An Empirical Valence Bond Approach for Comparing Reactions in Solutions and in Enzymes. J. Am. Chem. Soc 1980, 102, 6218–6226.(b)Warshel A Computer Modeling of Chemical Reactions in Enzymes and Solutions; John Wiley & Sons: New York, 1991.(c)Kamerlin SC; Warshel A The EVB as a quantitative tool for formulating simulations and analyzing biological and chemical reactions. Faraday Discuss. 2010, 145, 71–106. [PubMed: 25285029]

(19). Warshel A; Sharma PK; Kato M; Xiang Y; Liu H; Olsson MH Electrostatic basis for enzyme catalysis. Chem. Rev 2006, 106, 3210–3235. [PubMed: 16895325]

(20). (a)Ram Prasad B; Warshel A Prechemistry versus preorganization in DNA replication fidelity. Proteins: Struct., Funct., Genet 2011, 79, 2900–2919. [PubMed: 21905114] (b)Florian J; Goodman MF; Warshel A Computer simulations of protein functions: Searching for the molecular origin of the replication fidelity of DNA polymerases. Proc. Natl. Acad. Sci. U. S. A 2005, 102, 6819–6824. [PubMed: 15863620] (c)Florian J; Goodman MF; Warshel A Computer simulation studies of the fidelity of DNA polymerases. Biopolymers 2003, 68, 286–299. [PubMed: 12601790] (d)Florian J; Goodman MF; Warshel A Computer simulation of the chemical catalysis of DNA polymerases: Discriminating between alternative nucleotide insertion mechanisms for T7 DNA polymerase. J. Am. Chem. Soc 2003, 125, 8163–8177. [PubMed: 12837086]

(21). (a)Lee FS; Chu ZT; Warshel A Microscopic and Semimicroscopic Calculations of Electrostatic Energies in Proteins by the Polaris and Enzymix Programs. J. Comput. Chem 1993, 14, 161–185. (b)Warshel A; Chu ZT; Villa J; Strajbl M; Schutz CN; Shuriki A; Vicatos S; Chakrabarty S; Plotnikov NV; Schopf P Molaris-Xg, v9.11; 2012.

(22). Vicatos S; Rychkova A; Mukherjee S; Warshel A An effective Coarse-grained model for biological simulations: Recent refinements and validations. Proteins: Struct., Funct., Genet 2014, 82, 1168–1185. [PubMed: 25050439]

(23). (a)Kamerlin SCL; McKenna CE; Goodman MF; Warshel A A Computational Study of the Hydrolysis of dGTP Analogues with Halomethylene-Modified Leaving Groups in Solution: Implications for the Mechanism of DNA Polymerases. Biochemistry 2009, 48, 5963–5971. [PubMed: 19391628] (b)Kamerlin SCL; Williams NH; Warshel A Dineopentyl phosphate hydrolysis: Evidence for stepwise water attack. J. Org. Chem 2008, 73, 6960–6969. [PubMed: 18729515] (c)Klahn M; Rosta E; Warshel A On the mechanism of hydrolysis of phosphate monoesters dianions in solutions and proteins. J. Am. Chem. Soc 2006, 128, 15310–15323. [PubMed: 17117884] (d)Rosta E; Klahn M; Warshel A Studies of the reaction mechanism of phosphate hydrolysis in the ras-GAP proteins and in aqueous model systems. Abstr. Pap.—Am. Chem. Soc 2006, 232, 804–804.

(24). Aaqvist J; Warshel A Calculations of Free-Energy Profiles for the Staphylococcal Nuclease Catalyzed Reaction. Biochemistry 1989, 28, 4680–4689. [PubMed: 2765507]

(25). (a)Matute R; Warshel A Computational study on the catalytic role of the magnesium ions in the active site of the DNA Polymerase beta. Abstr. Pap.—Am. Chem. Soc 2016, 251.(b)Matute RA; Yoon H; Warshel A Exploring the mechanism of DNA polymerases by analyzing the effect of mutations of active site acidic groups in Polymerase. Proteins: Struct., Funct., Genet 2016, 84, 1644–1657. [PubMed: 27488241] (c)Yoon H; Warshel A The control of the discrimination between dNTP and rNTP in DNA and RNA polymerase. Proteins: Struct., Funct., Genet 2016, 84, 1616–1624. [PubMed: 27480935]

(26). Singh D; Wang YB; Mallon J; Yang O; Fei JY; Poddar A; Ceylan D; Bailey S; Ha T Mechanisms of improved specificity of engineered Cas9s revealed by single-molecule FRET analysis. Nat. Struct. Mol. Biol 2018, 25, 347–354. [PubMed: 29622787]

(27). (a)Gong SZ; Yu HH; Johnson KA; Taylor DW DNA Unwinding Is the Primary Determinant of CRISPR-Cas9 Activity. Cell Rep. 2018, 22, 359–371. [PubMed: 29320733] (b)Raper AT; Stephenson AA; Suo Z Sharpening the Scissors: Mechanistic Details of CRISPR/Cas9 Improve

Functional Understanding and Inspire Future Research. J. Am. Chem. Soc 2018, 140, 11142–11152. [PubMed: 30160947] (c)Raper AT; Stephenson AA; Suo ZC Functional Insights Revealed by the Kinetic Mechanism of CRISPR/Cas9. J. Am. Chem. Soc 2018, 140, 2971–2984. [PubMed: 29442507] (d)Yang M; Peng S; Sun R; Lin J; Wang N; Chen C The Conformational Dynamics of Cas9 Governing DNA Cleavage Are Revealed by Single-Molecule FRET. Cell Rep 2018, 22, 372–382. [PubMed: 29320734]

(28). (a)Kamerlin SCL; Warshel A At the dawn of the 21st century: Is dynamics the missing link for understanding enzyme catalysis? Proteins: Struct., Funct., Genet 2010, 78, 1339–1375. [PubMed: 20099310] (b)Warshel A; Bora RP Perspective: Defining and quantifying the role of dynamics in enzyme catalysis. J. Chem. Phys 2016, 144, 180901. [PubMed: 27179464]

(29). (a)Matute RA; Yoon H; Warshel A Exploring the mechanism of DNA polymerases by analyzing the effect of mutations of active site acidic groups in Polymerase beta. Proteins: Struct., Funct., Genet 2016, 84, 1644–1657. [PubMed: 27488241] (b)Ram Prasad B; Kamerlin SCL; Florián J; Warshel A Prechemistry barriers and checkpoints do not contribute to fidelity and catalysis as long as they are not rate limiting. Theor. Chem. Acc 2012, 131, 1288.(c)Ram Prasad B; Warshel A Prechemistry versus preorganization in DNA replication fidelity. Proteins: Struct., Funct., Genet 2011, 79, 2900–19. [PubMed: 21905114]

(30). Giraudpanis MJE; Duckett DR; Lilley DMJ The Modular Character of a DNA Junction-Resolving Enzyme - a Zinc-Binding Motif in Bacteriophage-T4 Endonuclease-Vii. J. Mol. Biol 1995, 252, 596–610. [PubMed: 7563077]

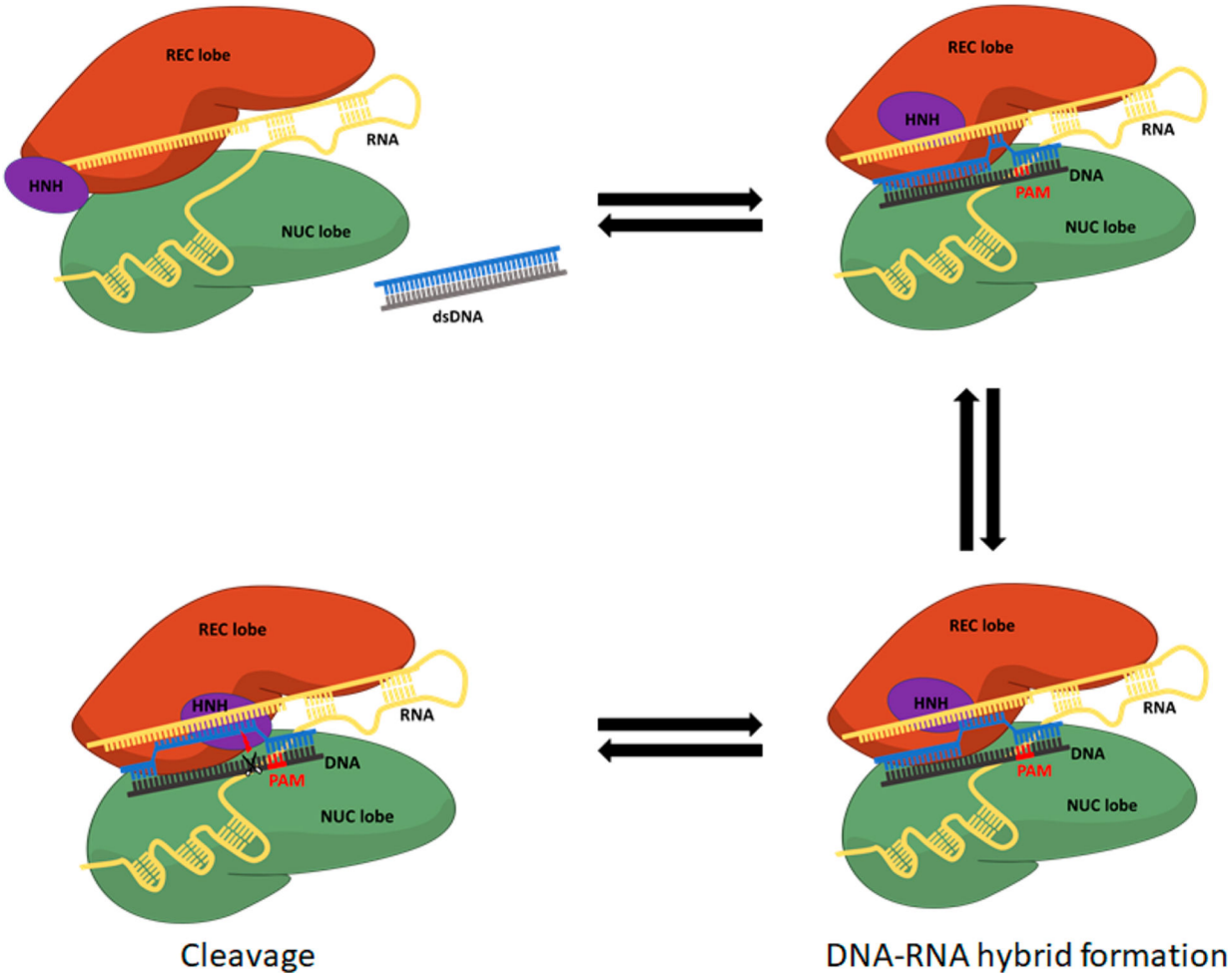

Figure 1.

The mechanism of the conformational change of Cas9 upon dsDNA binding and PAM recognition and cleavage. The structures of the PAM interacting domain and the guide are adjusted for PAM recognition, followed by DNA base pair melting and DNA–RNA hybridization. Then, the HNH domain undergoes rearrangement to bring catalytic residues to the cleavage site on the targeted DNA strand (phosphate at position −3).

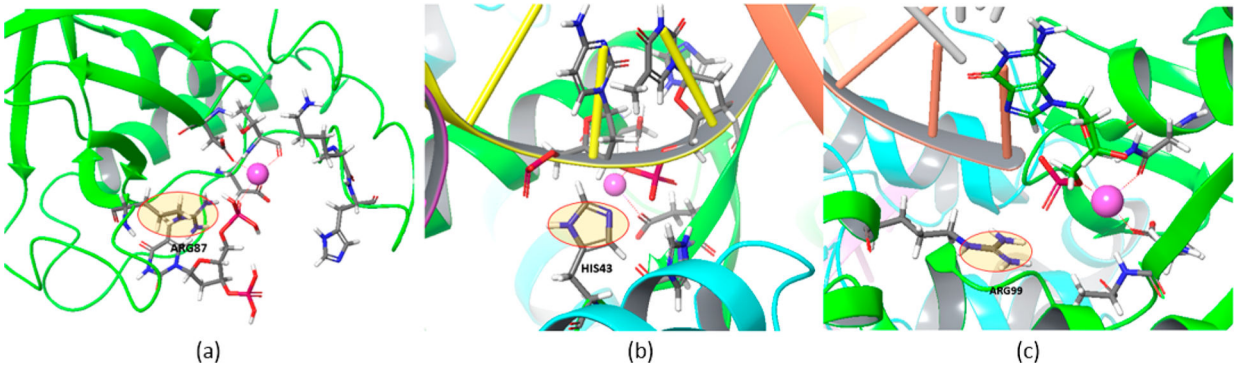

Figure 2.

Common positive residues (circled) at the catalytic site in (a) Staphylococcal nuclease, (b) T4 Endonuclease VII, and (c) Endonuclease Vvn.

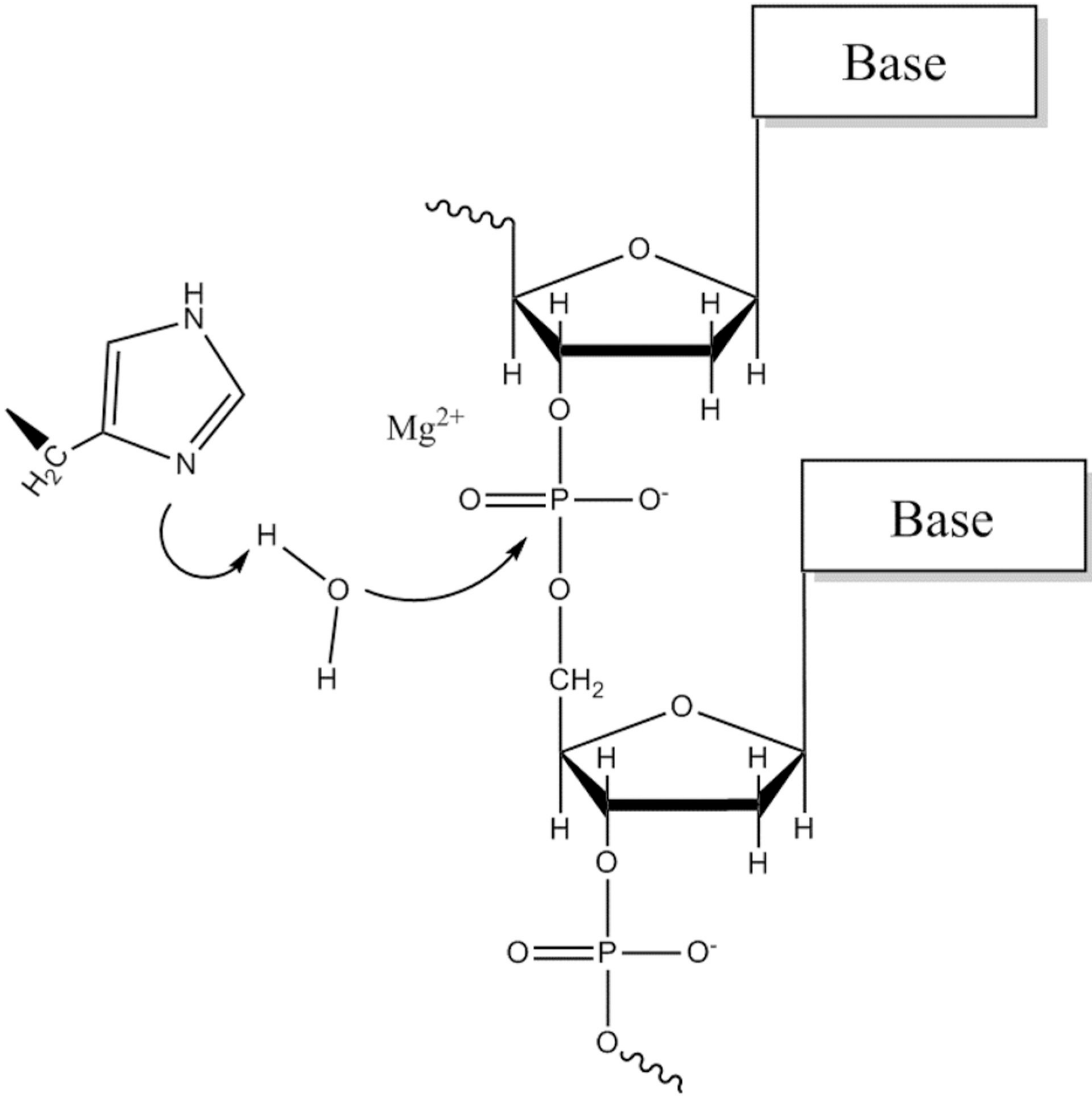

Figure 3.

One metal ion mechanism used in the calculation. A water molecule is deprotonated by N*δ* of histidine, and the resulting hydroxide ion attacks the scissile phosphate between two nucleotides.

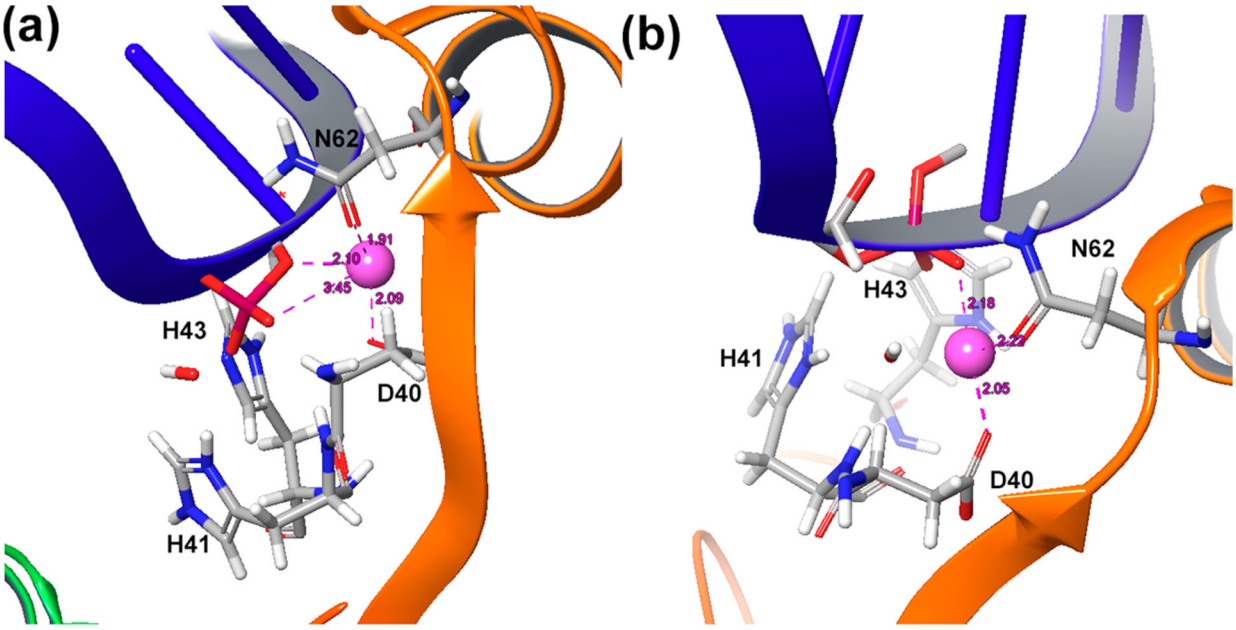

Figure 4.

Different positions of the Mg^{2+} ion in (a) the original crystal structure of Endo VII and (b) after adjusting it to favor the proton transfer step as well as the nucleophilic attack step.

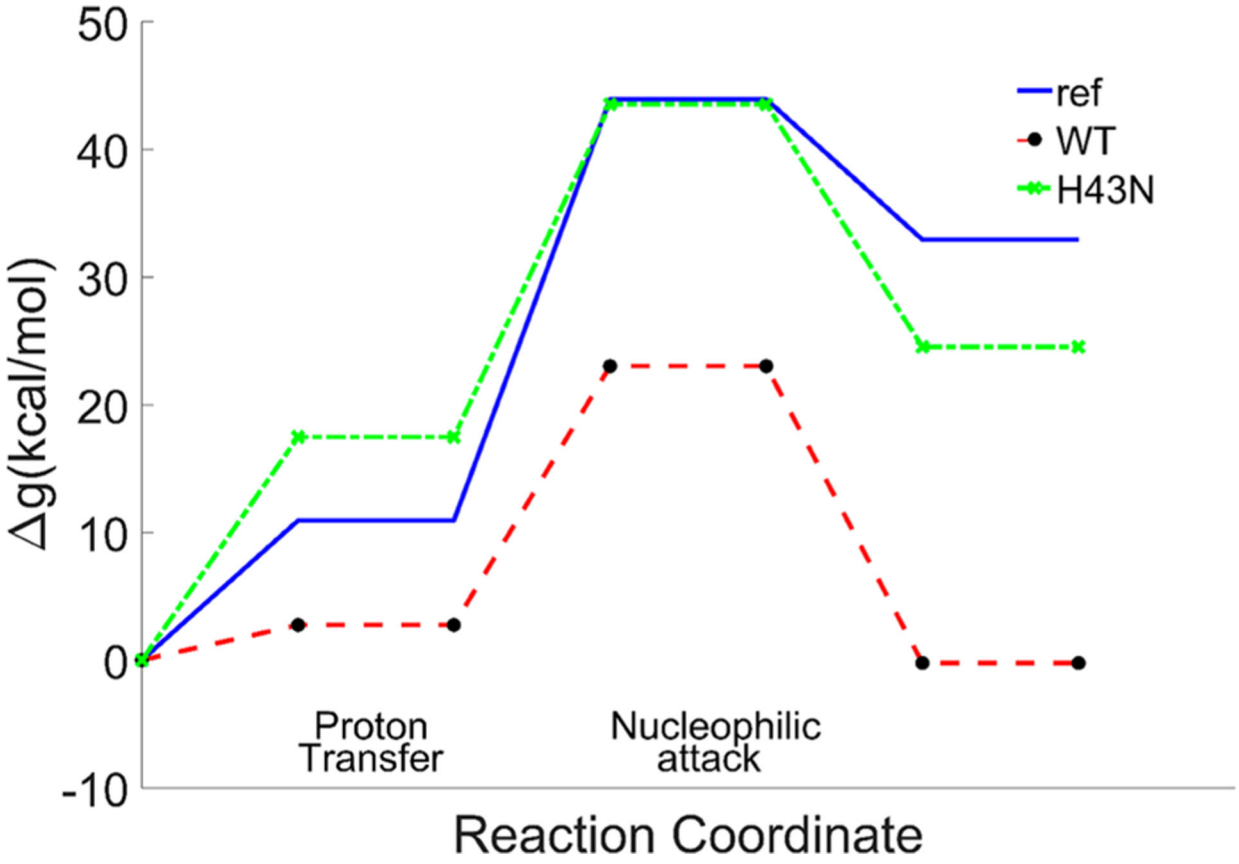

Figure 5.
Calculated free energy profiles for the reference reaction in solution, the wild type and H43N of Endo VII.

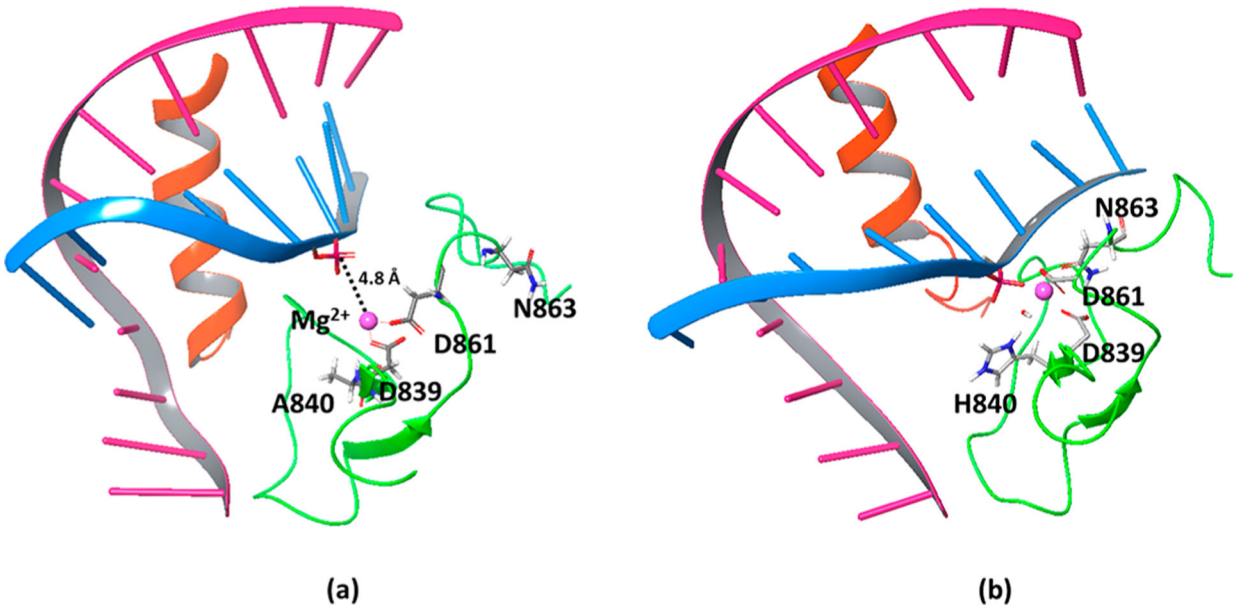

Figure 6.

(a) The Cryo-EM structure of Cas9 (PDB: 5Y36[8b]) where the catalytic H840 was mutated to alanine to stop the reaction. The distance between the scissile phosphate and the Mg^{2+} is 4.8 Å, and the N863 faces away from the catalytic site. (b) Adjusted Cas9 structure that brings HIS840 (converted from alanine) and ASN863 close to the corresponding positions in the catalytic site of Endo VII with a 3.3 Å distance between the scissile phosphate and the Mg^{2+}.

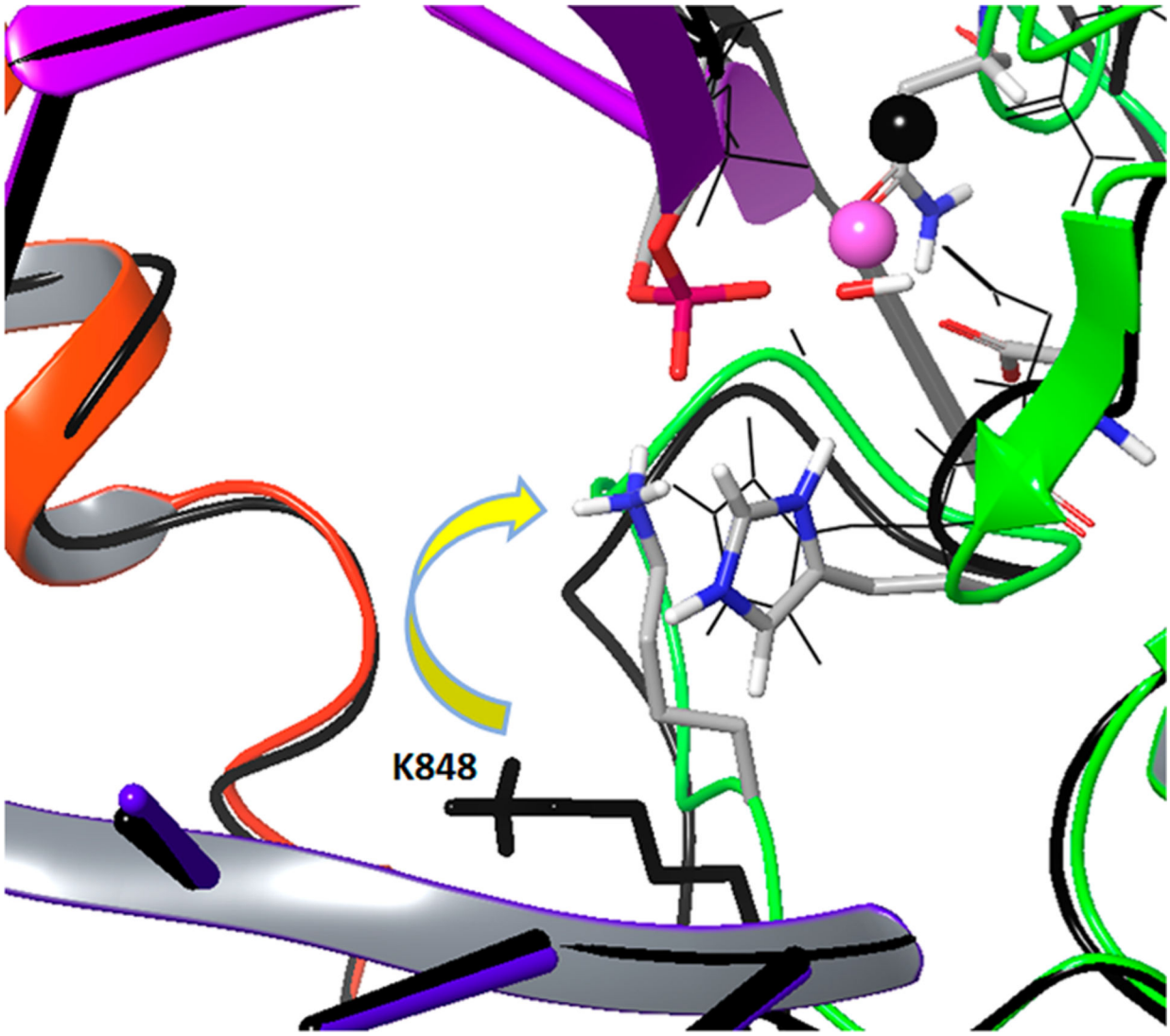

Figure 7.
Pulling K848 from its initial position (colored black) to the neighborhood of the scissile phosphate.

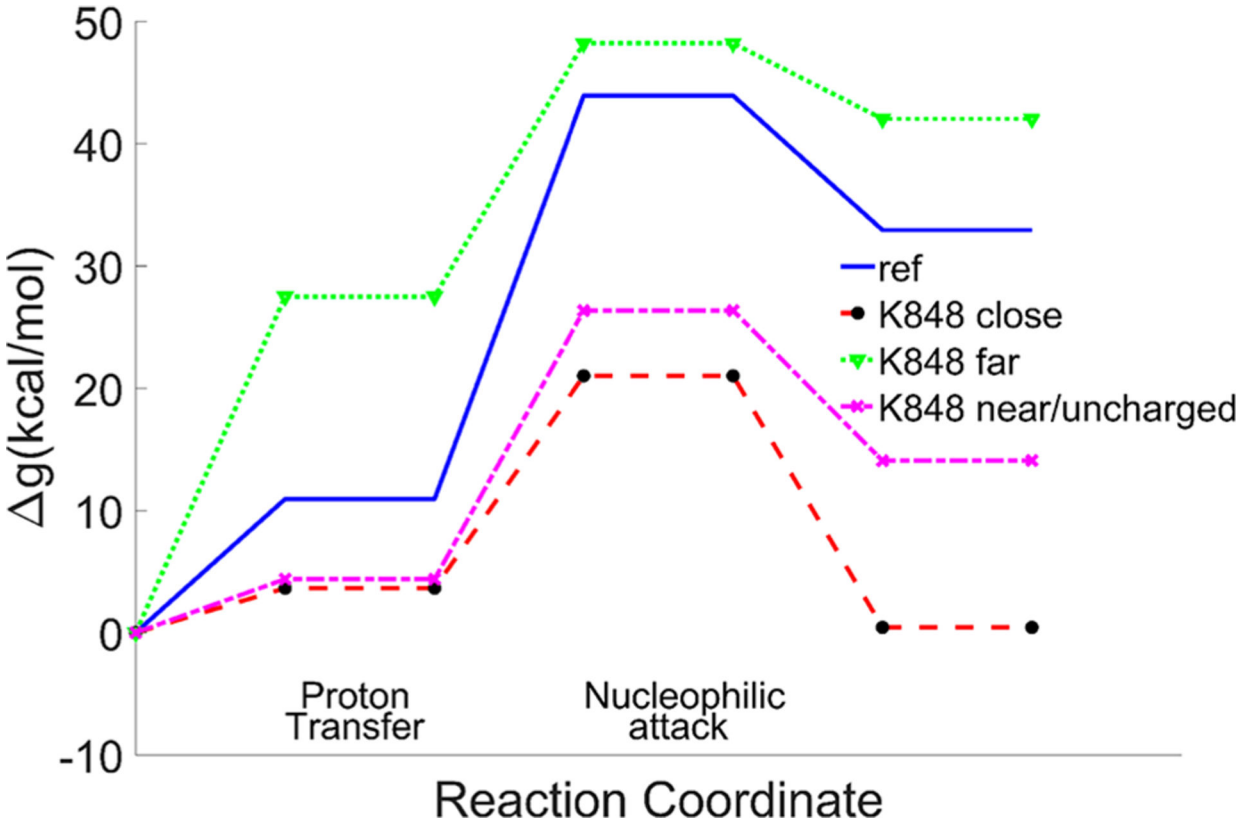

Figure 8.

EVB reaction profiles in the cases when K848 is far from the active site, and when it is near with/without being ionized. Note that the PT exotermicity is an integral part of the overall activation barrier.

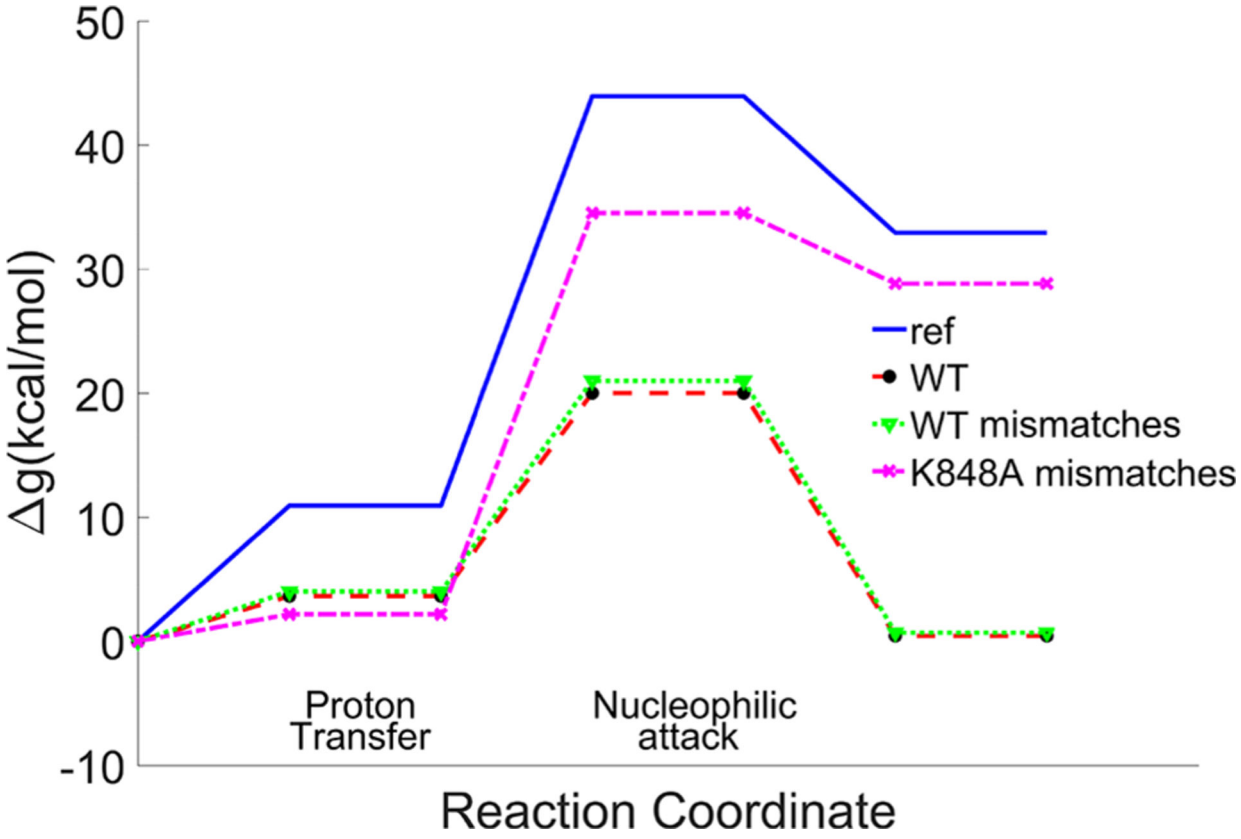

Figure 9.

EVB reaction profiles for Cas9 with and without three consecutive mismatch base parings from four nucleotides upstream of PAM. The effect of the mutation of K848 to alanine is also calculated. Note that the low barrier case is unlikely to occur, since the unwinding conformational change that leads to the K848 movement is unlikely to occur (see text). Note that the PT exotermicity is an integral part of the overall activation barrier.

Table 1.

Calculated Free Energy Profile for the Catalytic Reaction of T4 Endonuclease VII[a]

ref				wild type				H43N		
ΔG^{pt}	$\Delta g^{\ddagger,NA}$	$\Delta g^{\ddagger}$	$\Delta g^{\ddagger}_{obs}$	ΔG^{pt}	$\Delta g^{\ddagger,NA}$	$\Delta g^{\ddagger}$	$\Delta g^{\ddagger WT}_{obs}$	ΔG^{pt}	$\Delta g^{\ddagger,NA}$	$\Delta g^{\ddagger}$
10.93	33	43.93	43.93	2.75	20.40	23.02	21.48	17.47	26.05	41.12

[a]Free energies (kcal/mol) of the proton transfer (PT) step, the nucleophilic attack (NA) step, and the total barrier in the reference solution, the wild type, and the H43N mutant of Endo VII as well as the observed barrier converted from k_{cat} from ref 30.

Table 2.

Calculated Free Energy Profile for the Catalytic Reaction of Cas9 Different Systems[a]

ref				LYS848 far			LYS848 near/ionized			LYS848 near/un-ionized			
ΔG^{pt}	$\Delta g^{\ddagger,NA}$	$\Delta g^{\ddagger}$	$\Delta g^{\ddagger}_{obs}$	ΔG^{pt}	$\Delta g^{\ddagger,NA}$	$\Delta g^{\ddagger}$	ΔG^{pt}	$\Delta g^{\ddagger,NA}$	$\Delta g^{\ddagger}$	ΔG^{pt}	$\Delta g^{\ddagger,NA}$	$\Delta g^{\ddagger}$	$\Delta g^{\ddagger WT}_{obs}$
10.93	33	43.93	43.93	27.49	20.73	48.22	3.64	17.37	21.01	4.38	21.97	26.35	17.80

[a]Calculated free energies (kcal/mol) of proton transfer (PT) step, nucleophilic attack (NA) step, and total barrier in the reference solution and the three cases for Cas9. The observed barrier was converted from the k_{cat} of ref 26.